Conversion from citrate-stabilized amorphous calcium phosphate to nanocrystalline apatite: a surface-mediated solid-solid transformation

K. Chatzipanagis[a,§], M. Iafisco[b,§], T. Roncal-Herrero[a], M. Bilton[a,c], A. Tampieri[b], R. Kröger[c,*] and J. M. Delgado-López[d,e,*]

This work explores the role of citrate, an important component of the organic matrix of bone, in the crystallisation mechanism of amorphous calcium phosphate (ACP) in different aqueous media (i.e., pure water and PBS). Our results evidenced that citrate desorption triggered the ACP-to-Ap crystallisation, which occur through a surface-mediated solid-solid process. Considering that ACP is also widely used in biomedicine, the evaluation of its behaviour in aqueous media is very important for predicting their properties after their implantation *in vivo*.

Calcium phosphate (CaP) in the form of nanocrystalline apatite (Ap) is one of the most relevant biomineral since it constitutes the inorganic phase of bone, teeth and many pathological calcifications.[1, 2] Despite its importance, many aspects of the mechanisms behind the Ap formation remain nowadays under debate. In particular, the crystallization pathway, starting from an amorphous precursor, is still a matter of intensive research.[3-6] In fact, only in the last years, it was unequivocally demonstrated that in zebra fish bone[7] and in dental enamel[8], Ap formation does not occur directly by the association of ions from solution according to the classical nucleation and growth theory, but follows a "non-classical" crystallization pathway *via* an amorphous calcium phosphate (ACP) precursor. On this basis, the formation of ACP as a transient/intermediate phase is currently well accepted in *in vivo* bone mineralization.[9-11]

ACP to Ap conversion in aqueous solutions has been largely studied revealing that factors such as pH, temperature and presence of foreign ions (*i.e.* fluoride, magnesium, zinc, carbonates, silicates etc.) and additives (*i.e.* polyelectrolytes, phospholipids, polyglycols, proteins, etc.) affect the ACP stability and its transformation rate.[12, 13] This transformation has been proposed to occur, either directly from ACP to Ap or involving the formation of intermediate CaP phases (mostly octacalcium phosphate (OCP)), through different mechanisms:[12, 13] i) dissolution-reprecipitation; ii) clusters reorganization and, iii) solution-mediated solid-solid transformation. Therefore, it seems reasonable to assume that several processes might occur even simultaneously.

In this context, the role of citrate, in stabilizing the ACP has received less attention and only few reports can be found in the literature.[14-16] Citrate is an important component of mineralized tissues,[17] in fact in bone it accounts for ~2 wt%,[18] which is a concentration ~5-25 times higher compared to that occurring in the soft tissues (*i.e.* about 90% of the total citrate found in the body resides in bone).[17] In addition, recent NMR studies evidenced that it is strongly bound to the surface of bone Ap nanocrystals, controlling their shape and morphology.[19] However, its role in bone biomineralization is far from being clearly understood.

This work explores the crystallisation mechanism of citrate-functionalized ACP (cit-ACP) to Ap in different media, *i.e.* pure water and the physiological phosphate-buffer saline (PBS) solution. The morphological evolution of cit-ACP in aqueous solutions was studied by *ex situ* transmission electron microscopy (TEM), whereas the structural evolution was mainly monitored by *in situ* time-resolved Raman spectroscopy. It is noteworthy to mention that ACP not only plays a pivotal role in bone biomineralization but it is also a widely used biomaterial, being particularly relevant in medicine.[13] Hence, the evaluation of its behaviour in aqueous media is of paramount importance for predicting its properties after their possible implantation *in vivo*. Moreover, *in situ* characterization of ACP is rarely found in the literature mainly due to the transient characteristics of this phase, which is instantaneously transformed into a more stable crystalline phase.

Figure 1. *(A) Raman spectra of dry cit-ACP (red line) and Ap (blue line, obtained after 5 days of cit-ACP immersion in water). The vibrational modes involving phosphate groups are denoted in blue whereas those involving bonds of citrate are marked in red. Time-dependent Raman spectra collected during the transformation of cit-ACP in water (B) and in PBS (C).*

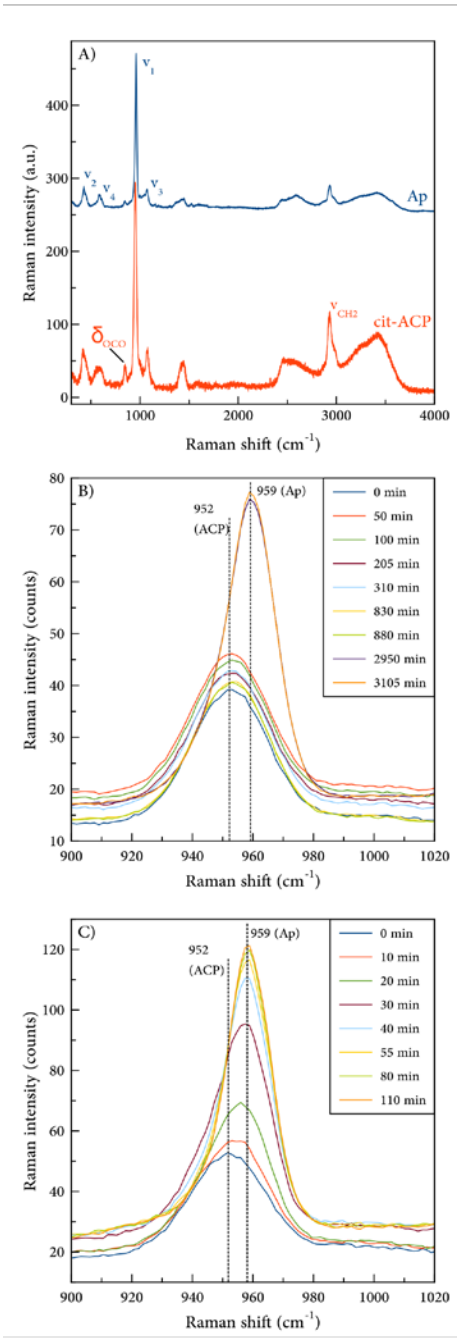

Dry powder cit-ACP was synthesized by the batch precipitation method described elsewhere.[14, 20, 21] (further information in S1, supplementary information). Figure 1A show the Raman spectra of cit-ACP particles. It exhibited bands related to the OCO bending (845-847 cm^{-1}), OCO stretching (1400-1600 cm^{-1}) and CH_2 stretching (2928-2933 cm^{-1}) modes of citrate.[20] In addition, phosphate vibrational modes are clearly visible in both spectra. Figure 1A also shows the Raman spectra obtained after immersing the cit-ACP particles in water during 5 days. The same citrate vibrations are still noticeable after the conversion to Ap (top spectrum in Fig. 1A) revealing that part of citrate is still attached to the inorganic phase even after phase transformation. The assignments of the corresponding vibrational modes are summarized in Table SP1 (supplementary information). The transformation process was studied *in situ* by monitoring the symmetric vibration of phosphate group (v_1PO_4). In water (Figure 1B), a single symmetric band centred at 952 cm^{-1} assignable to ACP[13, 22] was observed at the early stages. Upon maturation, this band progressively became asymmetric due to the formation of the crystalline Ap. Indeed, after 49 hours (2950 min), a distinct Raman peak at 959 cm^{-1} was observed. This value is in accordance with the Raman shift reported for nanocrystalline Ap.[20, 23] *In situ* time-dependent Raman spectra of cit-ACP immersed in PBS (Fig. 1C) clearly indicate that the cit-ACP-to-Ap conversion is greatly accelerated.

Figure 2. *Avrami fits to the data obtained in the case of pure PBS, a PBS/water mixture (1:1) and pure water. B) Plots of the linearized Avrami equation (ln[-ln(1-Φ)] vs ln(t)). Time derivative of the Avrami-fit (dΦ(t)/dt).*

The normalized ratio of the v_1PO4 Raman band, *i.e.* A_{959}/A_{952}, can be considered as the fraction of Ap/cit-ACP

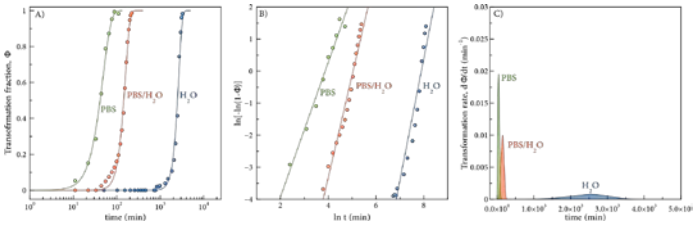

transformation, Φ. The time dependence of this transformation fraction is represented in Figure 2A. The sigmoidal curves shown in Fig. 2A are typical of solid-state reactions involving nucleation.[24] The induction time in PBS was 11 minutes whereas the tapering off period was reached after 110 minutes. On the other hand, the induction time in water was 830 minutes whereas the conversion gradually developed up to 3260 minutes, when the steady state was achieved. Thus, the appearance of Ap was significantly accelerated (by approximately 75 times) in PBS. As a control experiment we studied also the impact of a PBS/water mixture (1:1 volume) on the transformation kinetics (Fig. 2A), revealing an intermediate timescale for full transformation between that of pure water and PBS.

The kinetics of the cit-ACP-to-Ap transformation were studied in more detail using the Avrami model, which describes phase transformation in terms of volume fraction changes. This model is characterized by the generalized expression for the time dependence of the fraction of the transformed phase, Φ as[25, 26]

$$\Phi = 1 - \exp\left(-kt^n\right)$$

where the parameter *k* entails information on nucleation density and growth rates whereas *n* represents the dimensionality of the growth and the possible impact of diffusion. We assume here that $A_{959(Ap)}/A_{952(cit\text{-}ACP)} \propto \Phi$ upon complete transformation $\Phi = 1$ which means

that the data were normalized. However, the data reveal that signal of $\nu_{1(cit\text{-}ACP)}$ never completely vanishes indicating that an amorphous/disordered layer remains at the crystallite surface even after full crystallization, as previously proposed.[14, 15, 20, 27-29] The solid lines in Fig. 2A represent Avrami fits to the data obtained in the case of pure PBS, PBS/water mixture (1:1 volume) and pure water. A plot of ln[-ln(1-□□] *vs* ln(t) as shown in Fig. 2B reveals how closely the transformation follows Avrami kinetics (in comparison to the straight line fits shown in the figure). Overall we observed an approximate - albeit not perfect - fit of the data to an Avrami type kinetics with a goodness of fit varying between 97% and 99%. In particular, the transformation in PBS is indicative for an Avrami transformation, whereas for an increasing amount of water in the medium the initial parts of the curves show a changing slope during the transformation indicating an enhanced role of a change of nucleation rates during the process. This difference can be explained by the approximations made in the Avrami equation, namely assuming spherical crystal growth and ignoring diffusion and a time dependence of the nucleation. The slope of the lines provides information on the parameter *n* which differs significantly between the three cases and increase with increasing water content. We find values of *n* = 2.2, 3.2 and 3.9 for pure PBS, PBS/water and pure water, respectively. Assuming interface controlled phase transformation Wong and Czernuszka[30] relate values of *n* above 3 to either zero nucleation (*n*=3), decreasing nucleation rate (*n* = 3-4) or constant nucleation rate (*n* = 4) for solvent mediated re-dissolution and re-crystallisation processes and values below 3 indicate diffusion controlled growth. Hence, in PBS our observations suggest a significant role of species diffusion in solution leading to a rapid crystal growth. To evaluate the corresponding transformation rates the time derivative of the Avrami-fit $d\Phi(t)/dt$ was determined for cit-ACP transformation in the three media (shown in Fig. 2C). This plot reveals a rapid transformation for pure PBS with a maximum transformation rate of 2.0 10^{-2} min^{-1} which reduces to 1.0 10^{-2} min^{-1} and 1.2 10^{-3} min^{-1} for PBS/water and water, respectively. Hence, the maximum transformation rate roughly scales with the phosphate content in solution.

The morphological amorphous-to-crystalline evolution was studied by ex-situ High-resolution Transmission electron microscopy (HRTEM) and selected area electron diffraction (SAED). Figure 3A and B show the TEM micrographs of the as-prepared cit-ACP nanoparticles and the corresponding selected area electron diffraction (SAED) patterns, respectively. The particles, amorphous in nature as identified by the SAED, were round shaped with average diameters of 50 nm, as previously reported.[14, 15] In both media, only Ap phase was observed once the full transformation occurred (Figures 3e and f). However, we found different trends at the early stages. In water, the partial dissolution of the ACP was observed after one day (Fig. 3d), when the conversion already started. This was not observed in PBS. On the contrary, we found the appearance of crystalline domains within the cit-ACP (Fig. 3c). The SAED pattern collected from these domains indicates that they are crystalline apatite (STM card file no. 09-432). Similar domains have been previously observed by HRTEM during the ACP-to-Ap transformation.[31] In addition, the crystallisation of Ap from multiple nuclei within the primary ACP nanoparticles has been already proposed.[14] The complete dissolution of ACP before Ap crystallisation can be excluded as suggested by Raman results and by the time-lapse video recorded during the transformation (movie S1, supplementary material).

Figure 3. *(A,B) TEM micrograph of the as-prepared dry cit-ACP and the corresponding SAED. The morphological evolution of the particles immersed in PBS (left) and in water (right) are also shown. Note that the SAED pattern shown in panel C corresponds to the dark spots of the figure.*

The hydrolysis of ACP has been proposed to be the responsible for triggering the transformation of dry ACP to Ap in aqueous environment.[32] However, in the case of cit-ACP,

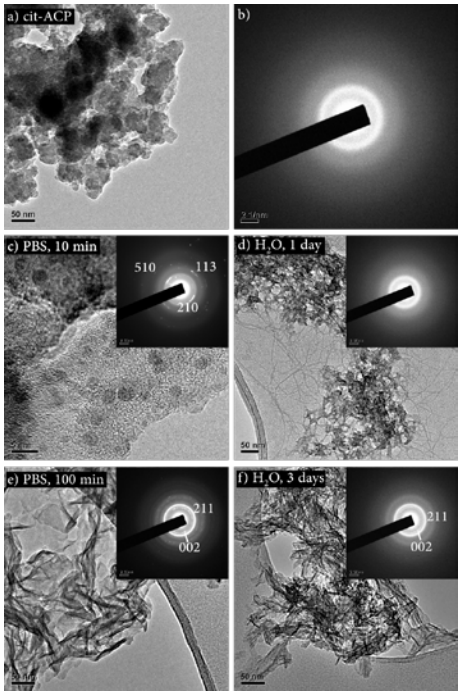

adsorbed citrate, blocking the surface active sites, inhibits this instantaneous transformation. We found that the intensity of the citrate δ_{OCO} Raman peak dramatically decreased at the early stages in both media (Fig. 4). Hence, the citrate desorption is the rate-determining step for the transformation to the crystalline phase. The left arrows in Fig. 4A and B indicate the induction time of the cit-ACP-to-Ap conversion. In PBS media the crystallisation starts soon after most of the citrate is released, whereas in water a longer time after the initial citrate desorption is required. After citrate desorption, the aqueous phosphate ions of PBS are exchanged with surface labile ions (*e.g.*, Cit^{3-} and HPO_4^{2-}) of cit-ACP, which would dramatically accelerate the transformation to Ap. A structural rearrangement of this labile surface layer could also explain the significant delivery of Ca^{2+} ions.[33]

Figure 4. *Time-dependent evolution of the normalized Raman peak of citrate (A(δ_{OCO})/A(ν_1PO_4)) in water (A) and PBS (B). The arrows indicate the induction times (left) and the times required for the total transformation (right) in each media.*

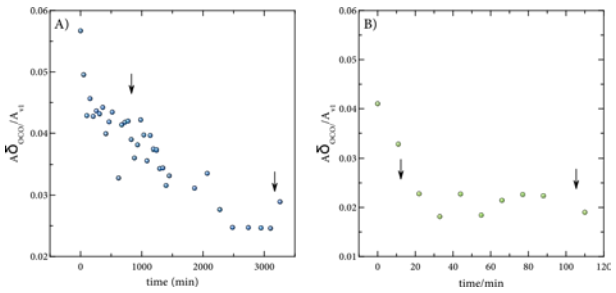

Conclusions

The combination of *ex situ* (TEM and SAED) and *in situ* (time-dependent Raman spectroscopy) experiments allowed monitoring the transformation of dry cit-ACP to Ap in two relevant media, *i.e.* ultrapure water and PBS. Our findings demonstrate that ACP directly transforms to Ap without involving the formation of any other intermediate CaP phase. We found out that citrate desorption triggered the cit-ACP crystallisation, which occur through a surface-mediated solid-solid process, involving the ionic-exchange between labile ions from ACP surface and the aqueous ions of the media. Indeed, the presence of phosphate in the media greatly accelerates such conversion (by approximately 75 times) as determined by *in situ* Raman spectroscopy. Although we cannot completely confirm the existence of an ionic rearrangement as the responsible of the ACP-to-crystalline conversion, on the basis of our results, a complete dissolution/re-precipitation mechanism can be completely excluded.

Notes and references

§ Both authors equally contributed to this work.

1. H. A. Lowenstam and S. Weiner, *On Biomineralization*, University Press, Oxford, 1989.
2. J. Gómez-Morales, M. Iafisco, J. M. Delgado-López, S. Sarda and C. Drouet, *Prog. Cryst. Growth Ch.*, 2013, **59**, 1-46.
3. H. Pan, X. Y. Liu, R. Tang and H. Y. Xu, *Chem. Commun.*, 2010, **46**, 7415-7417.
4. A. Selmani, I. Coha, K. Magdic, B. Colovic, V. Jokanovic, S. Segota, S. Gajovic, A. Gajovic, D. Jurasin and M. Dutour Sikiric, *CrystEngComm*, 2015, **17**, 8529-8548.
5. X. Niu, L. Wang, F. Tian, L. Wang, P. Li, Q. Feng and Y. Fan, *J Mech Behav Biomed Mater*, 2016, **54**, 131-140.
6. S. Jiang, Y. Chen, H. Pan, Y.-J. Zhang and R. Tang, *Phys. Chem. Chem. Phys.*, 2013, **15**, 12530-12533.
7. J. Mahamid, B. Aichmayer, E. Shimoni, R. Ziblat, C. Li, S. Siegel, O. Paris, P. Fratzl, S. Weiner and L. Addadi, *Proc. Natl. Acad. Sci. USA*, 2010, **107**, 6316-6321.
8. E. Beniash, R. A. Metzler, R. S. K. Lam and P. U. P. A. Gilbert, *J. Struct. Biol.*, 2009, **166**, 133-143.
9. L. B. Gower, *Chem. Rev.*, 2008, **108**, 4551-4627.
10. S. Weiner, J. Mahamid, Y. Politi, Y. Ma and L. Addadi, *Front. Mater. Sci. China*, 2009, **3**, 104-108.
11. F. Nudelman, K. Pieterse, A. George, P. H. H. Bomans, H. Friedrich, L. J. Brylka, P. A. J. Hilbers, G. de With and N. Sommerdijk, *Nat. Mater.*, 2010, **9**, 1004-1009.
12. S. V. Dorozhkin, *Acta Biomater.*, 2010, **6**, 4457-4475.
13. C. Combes and C. Rey, *Acta Biomater.*, 2010, **6**, 3362-3378.
14. J. M. Delgado-López, R. Frison, A. Cervellino, J. Gómez-Morales, A. Guagliardi and N. Masciocchi, *Adv. Funct. Mater.*, 2014, **24**, 1090-1099.
15. M. Iafisco, G. B. Ramirez-Rodriguez, Y. Sakhno, A. Tampieri, G. Martra, J. Gomez-Morales and J. M. Delgado-Lopez, *CrystEngComm*, 2015, **17**, 507-511.
16. Y. Chen, W. Gu, H. Pan, S. Jiang and R. Tang, *CrystEngComm*, 2014, **16**, 1864-1867.
17. R. L. Hartles, *Adv. Oral Biol.*, 1964, **1**, 225-253
18. E. Davies, K. H. Müller, W. C. Wong, C. J. Pickard, D. G. Reid, J. N. Skepper and M. J. Duer, *Proc. Natl. Acad. Sci. USA*, 2014, **111**, E1354-E1363.
19. Y. Y. Hu, A. Rawal and K. Schmidt-Rohr, *Proc. Natl. Acad. Sci. USA*, 2010, **107**, 22425-22429.
20. J. M. Delgado-López, M. Iafisco, I. Rodríguez, A. Tampieri, M. Prat and J. Gómez-Morales, *Acta Biomater.*, 2012, **8**, 3491-3499.
21. A. López-Macipe, J. Gómez-Morales and R. Rodríguez-Clemente, *Adv. Mater.*, 1998, **10**, 49.
22. G. B. Ramírez-Rodríguez, J. M. Delgado-López and J. Gómez-Morales, *CrystEngComm*, 2013, **15**, 2206-2212.
23. C. P. Tarnowski, M. A. Ignelzi and M. D. Morris, *J. Bone Miner. Res.*, 2002, **17**, 1118-1126.
24. A. L. Boskey and A. S. Posner, *J. Phys. Chem.*, 1973, **77**, 2313-2317.
25. M. Avrami, *J. Chem. Phys.*, 1941, **9**, 177-184.
26. M. C. Weinberg, D. P. Birnie Iii and V. A. Shneidman, *Journal of Non-Crystalline Solids*, 1997, **219**, 89-99.
27. Y. Sakhno, L. Bertinetti, M. Iafisco, A. Tampieri, N. Roveri and G. Martra, *J. Phys. Chem. C*, 2010, **114**, 16640-16648.
28. Y. Wang, S. Von Euw, F. M. Fernandes, S. Cassaignon, M. Selmane, G. Laurent, G. Pehau-Arnaudet, C. Coelho, L. Bonhomme-Coury, M.-M. Giraud-Guille, F. Babonneau, T. Azaïs and N. Nassif, *Nat. Mater.*, 2013, **12**, 1144-1153.
29. M. Duer and A. Veis, *Nat. Mater.*, 2013, **12**, 1081-1082.
30. A. T. C. Wong and J. T. Czernuszka, *Colloids Surf. A*, 1993, **78**, 245-253.
31. C.-G. Wang, J.-W. Liao, B.-D. Gou, J. Huang, R.-K. Tang, J.-H. Tao, T.-L. Zhang and K. Wang, *Cryst. Growth Des.*, 2009, **9**, 2620-2626.
32. S. Somrani, M. Banu, M. Jemal and C. Rey, *J. Solid State Chem.*, 2005, **178**, 1337-1348.
33. C. Rey, C. Combes, C. Drouet, S. Cazalbou, D. Grossin, F. Brouillet and S. Sarda, *Prog. Cryst. Growth Ch.*, 2014, **60**, 63-73.